

Strong coupling at room temperature in ultracompact flexible metallic microcavities

C. Grossmann, G. Christmann, J. J. Baumberg, I. Farrer, H. Beere et al.

Citation: *Appl. Phys. Lett.* **102**, 011118 (2013); doi: 10.1063/1.4773881

View online: <http://dx.doi.org/10.1063/1.4773881>

View Table of Contents: <http://apl.aip.org/resource/1/APPLAB/v102/i1>

Published by the [American Institute of Physics](#).

Related Articles

Realization of In_{0.75}Ga_{0.25}As two-dimensional electron gas bilayer system for spintronics devices based on Rashba spin-orbit interaction

J. Appl. Phys. **112**, 113711 (2012)

Characterization of InSb quantum wells with atomic layer deposited gate dielectrics

Appl. Phys. Lett. **101**, 233503 (2012)

Band structure calculations of InP wurtzite/zinc-blende quantum wells

J. Appl. Phys. **112**, 103716 (2012)

Temperature dependent band offsets in PbSe/PbEuSe quantum well heterostructures

Appl. Phys. Lett. **101**, 172106 (2012)

Polariton emission characteristics of a modulation-doped multiquantum-well microcavity diode

Appl. Phys. Lett. **101**, 131112 (2012)

Additional information on *Appl. Phys. Lett.*

Journal Homepage: <http://apl.aip.org/>

Journal Information: http://apl.aip.org/about/about_the_journal

Top downloads: http://apl.aip.org/features/most_downloaded

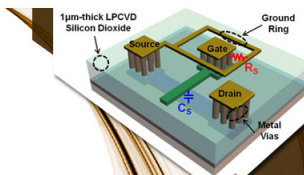
Information for Authors: <http://apl.aip.org/authors>

ADVERTISEMENT



**EXPLORE WHAT'S
NEW IN APL**

SUBMIT YOUR PAPER NOW!



SURFACES AND INTERFACES

Focusing on physical, chemical, biological, structural, optical, magnetic and electrical properties of surfaces and interfaces, and more...



ENERGY CONVERSION AND STORAGE

Focusing on all aspects of static and dynamic energy conversion, energy storage, photovoltaics, solar fuels, batteries, capacitors, thermoelectrics, and more...

Strong coupling at room temperature in ultracompact flexible metallic microcavities

C. Grossmann,¹ G. Christmann,¹ J. J. Baumberg,^{1,a)} I. Farrer,² H. Beere,² and D. A. Ritchie²

¹Nanophotonics Centre, Cavendish Laboratory, University of Cambridge, Cambridge CB3 0HE, United Kingdom

²Semiconductor Physics Group, Cavendish Laboratory, University of Cambridge, Cambridge CB3 0HE, United Kingdom

(Received 20 November 2012; accepted 16 December 2012; published online 8 January 2013)

Strong coupling between metallic microcavity modes and inorganic quantum well (QW) excitons at room temperature is observed in an ultracompact flexible sample design less than 100 nm thick. Four GaAs QWs embedded in a 65 nm AlGaAs/GaAs cavity are sandwiched between gold mirrors. The strong electromagnetic confinement and metallic phase shifts provide substantial local field enhancement and angular-resolved reflectivity spectra clearly show the anti-crossing in the dispersion relation resolving a Rabi splitting of 21 meV at room temperature, in good agreement with calculations. Flex-tuning metal thin foil microcavities demonstrate new possibilities for tunable optoelectronics and the study of polaritonic micromechanical effects. © 2013 American Institute of Physics. [<http://dx.doi.org/10.1063/1.4773881>]

Coupling light and matter within nanostructures is a thriving field of research for both fundamental physics and technological applications. Photons coupled to emitting quasiparticles such as excitons, plasmons, phonon-polaritons, single atoms, or molecules have been studied since the discovery of the Purcell effect.^{1–4} In planar microcavities based on Fabry-Perot designs, it is possible to situate organic or inorganic emitters with sub-nm accuracy at the positions of maximum electromagnetic field strength, creating strong interactions with potential for low power consumption light sources.⁵ The light-matter interaction can reach the strong coupling domain when mixing of the fundamental optical mode and the electronic transition, usually quantum well (QW) excitons, create new eigenstates termed cavity polaritons, whose coupling strength is described by the vacuum Rabi splitting, Ω_{Rabi} . These interacting bosons show unusual coherence properties and extreme stimulated nonlinear effects.^{6–10}

In order to reach strong coupling, the system either has to have low optical losses (long photonic lifetime) or large light-matter coupling. These control the Rabi splitting, $\Omega_{Rabi} \sim \sqrt{\Gamma \cdot N_{QW}/V}$, where N is the number of quantum wells, V is the spatial extent of the optical mode, and Γ is the free exciton decay rate which scales with the exciton oscillator strength.¹¹ For effective strong-coupling at room temperature, optimization of the exciton-photon coupling is possible using the large oscillator strength and binding energy excitons in gallium nitride or zinc oxide based semiconductors.^{12,13} Despite great efforts in fabrication, these structures still suffer from lower optical quality and electrical performance compared to GaAs systems which remain the inorganic paradigm system for low temperature strong-coupling experiments. Organic semiconductors show even larger oscillator strength, however, these materials lack durability due to irreversible bleaching on irradiation.

Critical to all these structures are ultra-high quality mirrors, usually distributed Bragg reflectors, which reflect more

than 99% of the incoming light. Their fabrication is time-consuming and requires many compromises in material selection making these structures bulky and expensive. An alternative approach to increase the exciton-photon coupling is to confine the light more tightly. A shorter effective cavity length (including mirror penetration which is typically on the order of several μm) produces larger Rabi splittings.¹¹ Stronger field confinement can be realized in metal-based semiconductor microcavities, where the mirror penetration depths for optical frequencies below the bandgap is on the order of only 10 nm leading to strong-coupling at room-temperature in ultracompact geometries.^{14,15} Further advantages of metallic mirrors include the capability of exciting localized plasmonic modes, which contribute additionally to the field confinement, as well as enabling direct electrical injection or field alignment of electronic states.^{16–18}

Here, we present an approach which combines the advantages of high-quality crystalline semiconductor cavities with the strong field confinement of metallic reflectors. Our hybrid structures are the most compact planar microcavity fabricated so far, and demonstrate how to optimally exploit confinement effects. Furthermore, because such ultra-thin layers are flexible, the additional strain degree of freedom allows investigation of the mechanical deformation of polariton devices at room temperature. Such miniaturized GaAs-based structures open up a range of potential applications, including sensors and flexible lasers.

Fabrication starts with a molecular beam epitaxial (MBE) grown multilayer of lattice-matched III–V material [Fig. 1(a)]. On top of the GaAs substrate is grown a 500 nm thick AlAs layer followed by a 65 nm thick $\text{Al}_{0.35}\text{Ga}_{0.65}\text{As}$ cavity containing four 5 nm thick GaAs quantum wells with 7 nm $\text{Al}_{0.35}\text{Ga}_{0.65}\text{As}$ barriers. Subsequently, we coat the cavity with 5 nm of TiO_2 , 200 nm of gold and add a layer of polyurethane and transparent polyethylene terephthalate (PET) foil on top which will act as the new flexible substrate [Fig. 1(b)]. In order to bond these layers together, the structure is heated up to 150 °C in a vacuum oven. Only the polyurethane

^{a)}Electronic address: jjb12@cam.ac.uk.

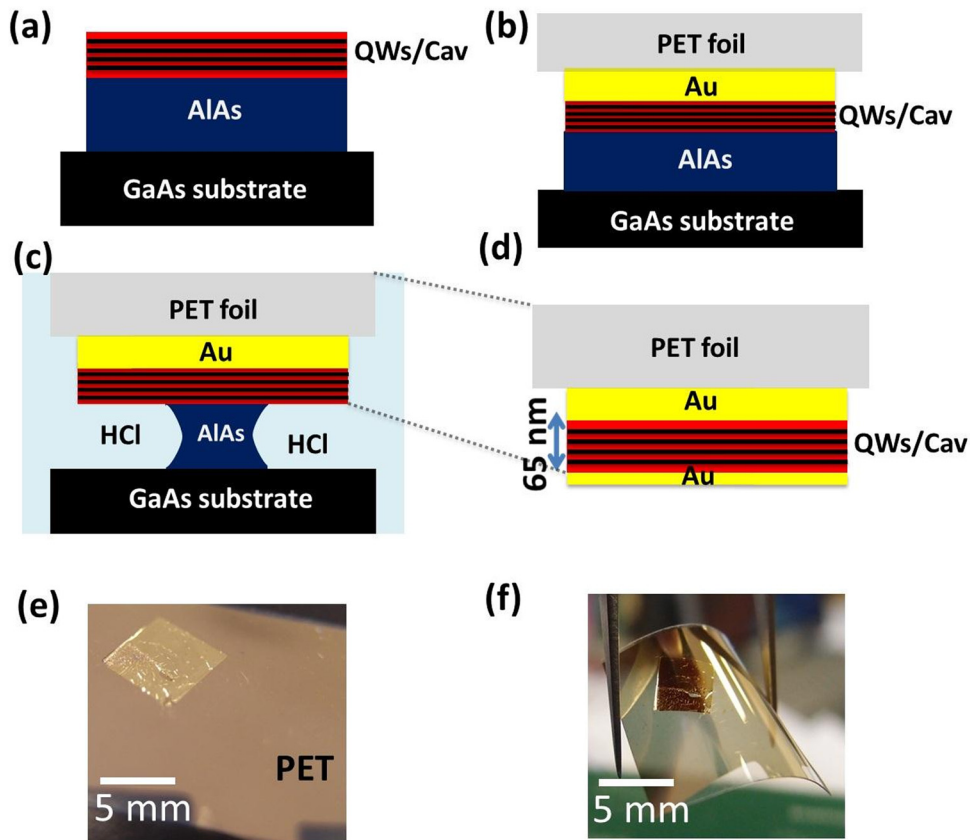


FIG. 1. Sample fabrication: (a) layer structure, (b) metal layer and PET substrate, (c) epitaxial lift-off by sacrificial wet etch, (d) complete cavity after epitaxial lift-off. (e) and (f) Photographs of final (e) and flexed (f) samples.

melts creating a solid air-bubble free bond between the PET foil and the rest of the sample. The structure is cooled down slowly to avoid intrinsic stress building up in the sample.

In order to access the other cavity facet, we epitaxially lift off the AlGaAs layer from the initial GaAs substrate via a wet etch of the AlAs in hydrochloric acid [Fig. 1(c)]. The selectivity of HCl etching for high Al-content allows the sacrificial removal of the AlAs layer while keeping the crystalline structure of the AlGaAs/GaAs cavity intact. The metallic half cavity on PET foil is subsequently rinsed and dried before a second 22 nm thick layer of gold [Fig. 1(d)] is evaporated on top in order to complete the cavity. The complete structure [Fig. 1(e)] can be reversibly deformed thanks to the resulting flexible substrate [Fig. 1(f)].

Stable optical modes in such ultra-compact subwavelength nanocavities are only possible because each metallic mirror reflection contributes phase shifts $\Delta\theta_{metal} = \pi + \frac{2n\omega}{\sqrt{\epsilon_b}\omega_p}$ to the round trip phase, with n the cavity refractive index, ω_p the gold plasma frequency, ϵ_b the background Au dielectric constant, and ω the mode eigenfrequency.¹⁹ Together with the contribution $\Delta\theta_{cav} = \frac{2nl\omega}{c}$ from the cavity length $l = 65$ nm (with c the vacuum velocity of light), the free-electron-like metal mirrors allow the lowest order resonance mode to fit into a cavity substantially shorter than the typical half wavelength design. The resulting 79 meV linewidth of the photonic mode is a balance between outcoupling and absorption, forming a cavity of quality factor $Q \approx 20$ which matches transfer matrix simulations.

The magnitude and spatial distribution of the intracavity field, computed with transfer matrix simulations, are plotted both before [Fig. 2(a)] and after [Fig. 2(c)] completion of the cavity showing that the local electromagnetic field more than

doubles in strength. We perform white light reflection spectroscopy in a confocal microscope configuration to confirm the intact GaAs QW absorption signatures in the half-cavity after epitaxial lift-off. In the reflectivity spectrum of Fig. 2(b), the highly reflective background of 200 nm gold overlays the heavy-hole (hh) and light-hole (lh) QW absorption dips, split by the 5 nm quantum confinement.

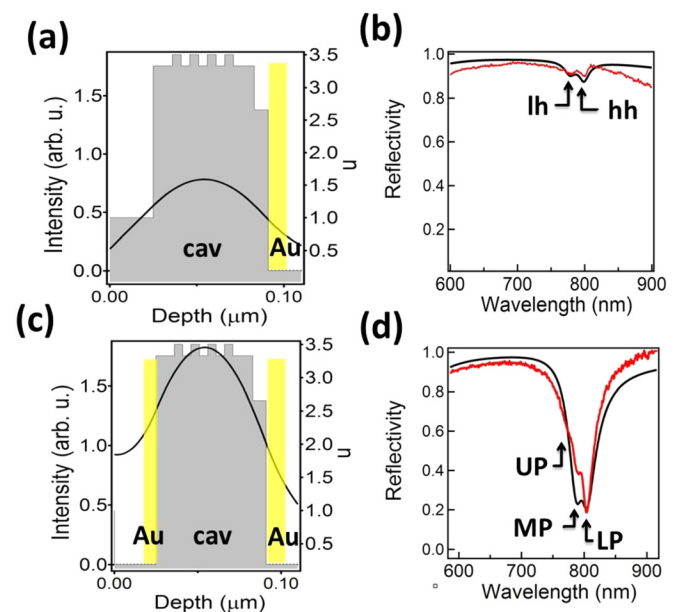


FIG. 2. (a) and (c) Intracavity field distributions (black line) and refractive index profiles (grey), with (b) and (d) simulated (red) and measured (black) white-light reflectivity spectra, for (a) and (b) half-cavity and (c) and (d) full cavity structures.

The spectra are completely transformed after completion of the cavity with the top Au layer [Fig. 1(d)]. We observe a triplet of modes [Fig. 2(d)], which correspond to the new eigenstates of the system, coupling metallic microcavity modes with QW excitons.

To locally characterise the dispersion coupling at each spatial position, angular-resolved reflectivity measurements are performed. A white light source illuminates the sample through a microscope objective of high numerical aperture $NA=0.9$ so that all the cavity modes with wave vector up to $k_{max} = \pm 6.8 \mu\text{m}^{-1}$ (limited by the NA) are simultaneously excited. The angles of incidence are selected in collection by laterally scanning across the reflected light a $125 \mu\text{m}$ core collection fiber coupled into a spectrometer at the back-focal plane of the objective, giving 5° angular resolution. We separately calibrate the detection angles which vary from 0° to 55° .

A set of TE-polarized reflectivity spectra for a typical region clearly show the photonic mode shifting to higher energies for increasing angles of incidence, approaching the hh QW exciton line at 796 nm [Fig. 3(a)]. For angles greater than 35° , the energy shift saturates and the QW-like dip starts to move away from the cavity mode. The transition is accompanied by a characteristic change in linewidth. This anticrossing behavior is a clear signature of strong coupling between the metallic microcavity mode and the QW excitons which form hybrid quasiparticles, the upper (UP), middle (MP), and lower (LP) polaritons with the two QW excitons. Extracting the mode energies allows comparison with a standard polariton coupling model which matches transfer matrix simulations (not shown) and resolves a Rabi splitting of 21 meV . This value is larger than in all other reports of strong coupling in GaAs-based structures both at room temperature and in Tamm plasmon polariton experiments carried out at cryogenic temperatures.^{15,20-22}

Another advantage of ultracompact metal microcavities fabricated by epitaxial lift-off is the freedom to select any new substrate. Combining MBE-grown crystals with flexible substrates opens unusual alternatives for manipulating polaritons in strongly coupled microcavities. By applying external

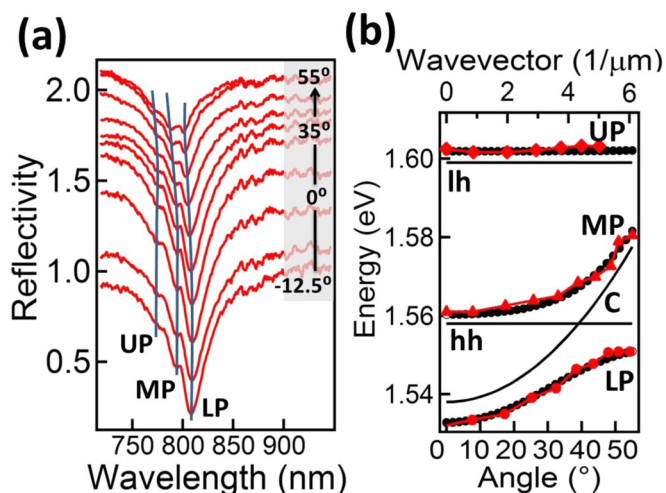


FIG. 3. (a) Angle-dependant reflectivity spectra (blue line is guide to eye). (b) Experimental dispersion curves (red markers) and model (black circles) of LP, MP, and UP. The uncoupled cavity mode (C) and exciton energies (hh, lh) are shown with black lines.

stress, it is possible to red- or blue-shift the exciton energy (depending on the experimental configuration) without compromising the exciton oscillator strength as in the case of the quantum confined Stark effect.²³

In order to monitor the influence of applied external strain, the sample is mounted on a microscope slide with an 8 mm diameter central hole [Fig. 4(a)]. The sample is aligned with the opening and rigidly clamped down onto the glass slide around the aperture circumference. Access to the sample backside allows positioning a $\approx 50 \mu\text{m}$ tip-diameter pin mounted on a 3-axis translation stage directly underneath it. Translating the pin upwards bends the sample [Fig. 4(a)], applying controllable strains while simultaneously reflectivity spectra are recorded. Typical spectra for increasing strain [Fig. 4(b)] show the evolution of the lowest polariton modes (at a slightly different location on the sample than Fig. 3). Initially, the hh exciton-like MP mode red-shifts, eventually matched only at larger strains by the cavity-like LP mode [Fig. 4(c)].

This behaviour can be explained by the elastic strain-induced change of the optical bandgap in the GaAs/AlGaAs quantum wells. The pin bends the flexible PET foil leading to a geometrical expansion of both the substrate and the gold/semiconductor multilayer as depicted in Fig. 4(a). In the elastic regime, this directly translates into a lattice expansion giving rise to a redshift of the exciton energy and hence the polariton modes. In order to estimate the magnitude of the strain-induced exciton energy shifts, we simulate the strained quantum well structure. From our geometry, we produce linear expansions of up to 10^{-3} assuming perfect bonding between the PET and the gold/semiconductor layers. However, the stress transfer at the interface between soft PET and rigid gold/AlGaAs can be estimated from the ratio of Young's moduli, $\frac{E_{PET}}{E_{gold}} = \frac{7 \text{ GPa}}{79 \text{ GPa}} \approx 0.1$.²⁴ The expected

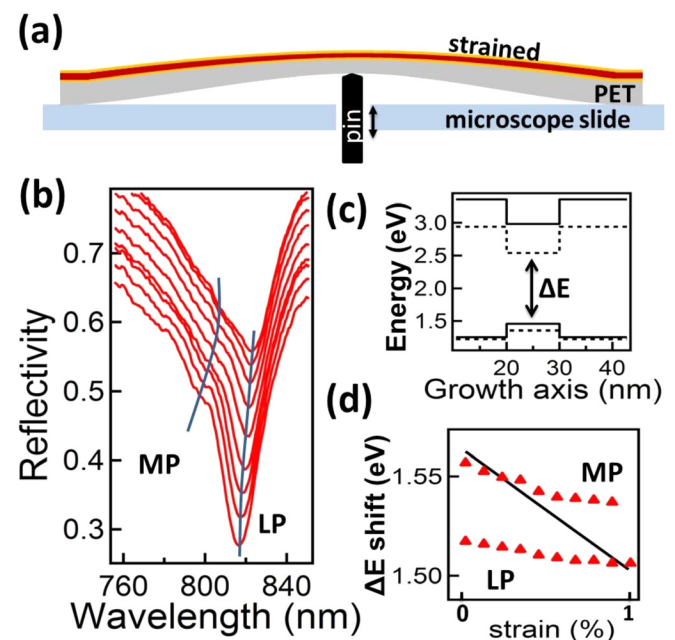


FIG. 4. (a) Strain setup and sample geometry. (b) White-light reflectivity spectra of strained structure. (c) Simulated bandgap of unstrained (solid line) and strained (dashed) AlGaAs/GaAs structure. (d) Experimental strain-induced shift of MP and LP (red markers) and simulated strain-induced bandgap change (black line).

bandgap shifts [Fig. 4(c)] (simulated with a Schroedinger-Poisson solver) give the modified exciton energies which compare well with the measurements [Fig. 4(d)], showing flex-induced tuning through the strong-coupling resonance.

In conclusion, we show a promising route towards strong light-matter interaction in ultracompact microcavities. Our innovative fabrication allows the realization of the smallest planar microcavity yet realized with a geometrical cavity length of just 65 nm. The extreme field confinement is evident in the largest value of Rabi-splitting ever measured in GaAs-based structures, at low and at room temperatures. The epitaxial lift-off approach facilitates novel mechanical deformations to study the light-matter interaction. Such thin foils can be reversibly deformed over many cycles. Due to the metallic mirrors, the lattice-matching conditions required for conventional MBE-grown semiconductor microcavities regarding reflector and cavity materials are circumvented. Localized photonic modes such as surface plasmons or waveguide modes can be easily incorporated within these devices in order to further boost the field confinement.

The authors acknowledge financial support from UK EPSRC EP/C511786/1, EP/F011393, Toshiba Ltd. and EU CLERMONT4 and INDEX. C.G. wants to thank P. Farah for invaluable help in the sample fabrication process.

¹C. Weisbuch, M. Nishioka, A. Ishikawa, and Y. Arakawa, *Phys. Rev. Lett.* **69**, 3314 (1992).

²See, e.g., R. Ameling and H. Giessen, *Nano Lett.* **10**, 4394 (2010), and references therein.

³K. Huang, *Proc. R. Soc. London, Ser. A* **208**, 352 (1951).

⁴*Cavity Quantum Electrodynamics*, edited by P. Berman (Academic, San Diego, 1994).

⁵J. L. Jewell, J. P. Harbinson, A. Scherer, Y. H. Lee, and L. T. Florez, *IEEE J. Quantum Electron.* **27**, 1332 (1991).

- ⁶P. G. Savvidis, J. J. Baumberg, R. M. Stevenson, M. S. Skolnick, D. M. Whittaker, and J. S. Roberts, *Phys. Rev. Lett.* **84**, 1547 (2000).
- ⁷J. Kasprzak, M. Richard, S. Kundermann, A. Baas, P. Jeambrun, J. M. L. Keeling, F. M. Marchetti, M. H. Szymanska, R. André, J. L. Staehli, V. Savona, P. B. Littlewood, B. Deveaud, and L. S. Dang, *Nature* **443**, 409 (2006).
- ⁸S. Christopoulos, G. Baldassarri Höger von Högersthal, A. J. D. Grundy, P. G. Lagoudakis, A. V. Kavokin, J. J. Baumberg, G. Christmann, R. Butté, E. Feltin, J.-F. Carlin, and N. Grandjean, *Phys. Rev. Lett.* **98**, 126405 (2007).
- ⁹A. Amo, D. Sanvitto, F. Laussy, D. Ballarini, E. del Valle, M. Martin, A. Lemaître, J. Bloch, D. Krizhanovski, M. Skolnick, C. Tejedor, and L. Vina, *Nature* **457**, 291 (2009).
- ¹⁰G. Tosi, G. Christmann, N. G. Berloff, P. Tsotsis, T. Gao, Z. Hatzopoulos, P. G. Savvidis, and J. J. Baumberg, *Nature Phys.* **8**, 190 (2012).
- ¹¹M. S. Skolnick, T. A. Fisher, and D. M. Whittaker, *Semicond. Sci. Technol.* **13**, 645 (1998).
- ¹²G. Christmann, R. Butte, E. Feltin, A. Mouti, P. A. Stadelmann, A. Castiglia, J.-F. Carlin, and N. Grandjean, *Phys. Rev. B* **77**, 085310 (2008).
- ¹³R. Schmidt-Grund, B. Rheinlinder, C. Czekalla, G. Benndorf, H. Hochmuth, M. Lorenz, and M. Grundmann, *Appl. Phys. B* **93**, 331 (2008).
- ¹⁴P. A. Hobson, W. L. Barnes, D. G. Lidzey, G. A. Gehring, and D. M. Whittaker, *Appl. Phys. Lett.* **81**, 3519 (2002).
- ¹⁵C. Grossmann, C. Coulson, G. Christmann, I. Farrer, H. Beere, D. A. Ritchie, and J. J. Baumberg, *Appl. Phys. Lett.* **98**, 231105 (2011).
- ¹⁶J. Bellessa, C. Bonnard, J. C. Plenet, and J. Mugnier, *Phys. Rev. Lett.* **93**, 036404 (2004).
- ¹⁷J. R. Tischler, M. C. Bradley, V. Bulović, J. H. Song, and A. Nurmikko, *Phys. Rev. Lett.* **95**, 036401 (2005).
- ¹⁸S. Hayashi, Y. Ishigaki, and M. Fujii, *Phys. Rev. B* **86**, 045408 (2012).
- ¹⁹M. Kaliteevski, I. Iorsh, S. Brand, R. A. Abram, J. M. Chamberlain, A. V. Kavokin, and I. A. Shelykh, *Phys. Rev. B* **76**, 165415 (2007).
- ²⁰T. R. Nelson, Jr., J. P. Prineas, G. Khitrova, H. M. Gibbs, J. D. Berger, J.-H. Shin, H.-E. Shin, Y.-H. Lee, P. Tayebati, and L. Javnskis, *Appl. Phys. Lett.* **69**, 3031 (1996).
- ²¹S. I. Tsintzos, P. G. Savvidis, G. Deligeorgis, Z. Hatzopoulos, and N. T. Pelekanos, *Appl. Phys. Lett.* **94**, 071109 (2009).
- ²²C. Symonds, A. Lemaître, P. Senellart, M. H. Jomaa, S. Aberra Guebrou, E. Homeyer, G. Brucoli, and J. Bellessa, *Appl. Phys. Lett.* **100**, 121122 (2012).
- ²³R. B. Balili, D. W. Snoke, L. Pfeiffer, and K. West, *Appl. Phys. Lett.* **88**, 031110 (2006).
- ²⁴L. S. Schadler and I. C. Noyan, *J. Mater. Sci. Lett.* **11**, 1067 (1992).